TRAINING SITE SELECTION BASED ON UNCERTAINTY ESTIMATION FOR OPTICAL SATELLITE IMAGE CLASSIFICATION

Yi-Shiang Shiu[1] and Chun-Jia Huang[2]
[1] Department of Urban Planning and Spatial Information, Feng-Chia University, No. 100, Wenhwa Rd., Seatwen Dist., Taichung, 40724 Taiwan
Email: ysshiu@fcu.edu.tw
[2] Department of Civil Engineering, National Chung Hsing University, No. 250, Kuo Kuang Road, South Dist., Taichung, 40227 Taiwan
Email: steven8549@gmail.com

KEY WORDS: weights of evidence, maximum likelihood classifier, pure pixel index, gray-level co-occurrence matrices

ABSTRACT: For image classification, it is crucial to derive a classifier from a limited training data which can be useful to classify other testing samples without over-fitting. In this study, we applied weights of evidence model to locate possible training areas which can be used to optimize the classification results. Agricultural area in Chiayi, Taiwan is chosen as the study area. We used SPOT-5 images and hybrid classifier to classify the land cover into two dominant classes in the study area: pineapple and non-pineapple. Gray-level co-occurrence matrices (GLCM) and pure pixel index (PPI) are assumed as the key spatial factors for uncertainty estimation and can help indicate the best training areas for image classification. The weights of evidence model (WoE) was used to combine the spatial factors to map the uncertainty estimation results. The receiver operating characteristics (ROC) with area under curve (AUC) calculation was used to evaluate the proposed model. Future applications include providing the best and minimum training sites and maximizing the accuracy of image classification.

1. INTROCUTION

Satellite image classification is considered to be the important process to extract land use / land cover information. Supervised classification needs training samples for the classification of the image. However, gathering training samples with representative information and excellent quality is a tough and time-consuming step. Training samples directly affect the quality of the classification. Therefore, developing an accurate, objective and automated extraction method of training sample can make image classification more effective.

Traditional training sample selection is based on artificial way which is subjective and result in error. Several automatic or semi-automatic extraction methods of training area have been developed to improve the accuracy of training sample and the efficiency of image classification. SAFTE (semi-automated training field extraction) was designed to automatically delineate training areas with only an initial "seed pixel" for each field and a set of user specified extraction parameters including maximum absolute summed variance, maximum size and maximum relative-variance-increase ratio for a field (Buchheim and Lillesand, 1989). Based on the concepts of SATFE, more studies combined unsupervised concepts (Skidmore, 1989), prior knowledge of geometric characteristics of land features (Bolstad and Lillesand, 1992; Hiroshi Okumuraa, 2003) or image segmentation (Mccaffrey and Franklin, 1993) to improve the consistency and efficiency of the extraction of training area. Similarly, some studies extracted part of the training sample area by calculating setting a threshold as the basis for classification (Ozdarici Ok and Akyurek, 2011). As the development of support vector machine (SVM), fewer training data sets are required to achieve higher classification accuracy compared with previous classifiers (Mantero et al., 2004). Therefore, more studies focused on designing approaches of training site selection suitable for SVM. For example, previous studies have proven that only the training samples lying on part of the edge of the class distribution in feature space are helpful for building support vectors; and thus, for crop classification, using ancillary soil information properly can help select the support vectors and reduce the amount of training sites significantly in the SVM classifier (Foody, 2008; Foody and Mathur, 2004). Another case is to combine spatial sampling schemes and use spatial statistics to compare information density of data to be classified with data used in the reference process (Mountrakis and Xi, 2013). Several approaches for endmember selection, on the other hand, were proposed and used to cooperate with spectral mixture analysis in order to identify spectral characteristics and mixed ratio of each pixel in a given hyperspectral image. Popular approaches including N-FINDR (Winter, 1999) and pixel purity index (PPI) (Boardman, 1994) were also applied to training site selection for image classification.

Although the previous studies above developed diverse methodology for various classifiers, they demonstrated a common concept—the purity and homogeneity of training sites dominates classification accuracy. Highly

homogeneous training sites usually contribute to good classification results (Shao and Lunetta, 2012). Generally, the common purpose for the related research above is to improve the degree of automation in the training field extraction while maintaining an acceptable level of classification accuracy. Current semi-automatic extraction methods of training sample area have been proved to be more efficient than the traditional extraction methods, manual and subjective selection of the initial seeds or thresholds is still necessary though. Besides, most approaches exhibited binary rather than continuous results and thus lacked the flexibility of training site selection for end users.

Uncertainty estimation provides continuous and spatial probability distribution and has been used in risk management and error analysis of image classification (Comber et al., 2012; Muñoz-Marí et al., 2012). For risk management, the most popular models are certainty factor (CF) and weights of evidence (WoE). Certainty factor (CF) model has been used to evaluate the reliability of the rules induced from the decision support system for risk mapping (Sinha and Zhao, 2008). Literature also proved that GIS-based spatial risk assessment with CF model can be beneficial for hazard susceptibility mapping (Aboye, 2009; Binaghi et al., 1998; Devkota et al., 2013; Lan et al., 2004; Pourghasemi et al., 2012). Similar as CF model, WoE is a quantitative model for combining evidence in support of a hypothesis and was originally developed for medical diagnosis rather than spatial analysis. Risk assessments of training sites (Dahal et al., 2008; Pourghasemi et al., 2012; Regmi et al., 2014) and flooding (Tehrany et al., 2014) are also the main applications of WoE.

The above instances demonstrate that risk assessment can help to delineate environmentally sensitive areas and has been widely used to investigate the probability of risk occurrence and evaluate risk levels for hazard prevention (Zhang et al., 2009). In this study, we used WoE model to map the areas prone to be suitable training sites. According to the common conclusions of the previous studies, we chose indexes which can represent the homogeneity of a given area as the factors for the WoE model.

2. DATA AND METHODS

2.1 Study Area and Data

We chose part of Minsyong Township, Chiayi County in the Central Taiwan as the study area (Fig.1). The study area is about 700 ha. Minsyong is a very good representative area of pineapple cultivation because it holds the top three yield and cultivation area in Taiwan during the five years. Wide and successive pineapple fields show up as homogeneous areas. However, a pineapple field exhibits mixed spectra because of the mixture of pineapple plants and soil, which increases the difficulty in training site selection. Therefore, pineapple cultivation areas are suitable for studying intelligent training site selection.

The satellite image we used is SPOT-5 supermode imagery with four bands and 2.5 m spatial resolution. The supermode imagery was generated from two panchromatic images acquired simultaneously at a resolution of 5 meters and offset vertically and horizontally by 2.5 meters. The acquisition date of the image was October 23rd, 2012. The image was orthorectified with the rational polynomial coefficient model of the SPOT-5 sensor. Besides, image-to-map registration with road network and cadastral parcel data was performed to yield a root mean square error (RMSE) of 0.5 pixels.

In order to match up the acquisition date of the satellite image, we surveyed the pineapple cultivation conditions of the study area on October 22nd, 2012. The results were recorded based on cadastral parcel data and show whether each parcel is a pineapple field or not. The accuracy of the survey data is about 95%. These data were used to choose training areas and for validation of the classification results.

2.2 Purity and Homogeneity Calculation

Since purity and homogeneity of training sites were proven to dominate classification accuracy, we assumed that PPI and gray-level co-occurrence matrices (GLCM) are the key indexes to represent these two kinds of characteristics respectively.

PPI is based on the geometry of convex sets in an *N*-dimensional space. First, a dimensionality reduction is applied to the original satellite image with minimum noise fraction (MNF) (Boardman, 1994; Ifarraguerri and Chein, 1999; Martínez et al., 2006). A large number of random *N*-dimensional vectors were generated and then every image data point was projected onto each vector. The image data points which correspond to extreme values in the direction of a vector were identified and placed on a list. Threshold factor can be the benchmark to choose the extreme pixels. For example, a value of 2 flags all pixels greater than two DN values from the extreme pixels (both high and low) as

extreme and would be placed on a list. As more vectors were generated, the list grew, and the number of times a given pixel was placed on this list was also tallied. Finally, the pixels with the highest tallies were considered as the purest ones. We set the number of iterations as 10,000 and the threshold factor as 5 separately; all pixels with tallies higher than zero were chosen as the training data of pure areas. Contrarily, the threshold factor was set as 40; all pixels with tallies equal to zero were selected as the training data of non-pure areas. The training data here only used for the logistic regression model mentioned as below.

GLCM and their application approaches on the satellite image in this study is based on the works of Haralick (1979) and Puissant et al. (2005). Compared to a simple statistical approach using mean or standard deviation, GLCM allows the incorporation of both spectral and spatial distribution of image gray values. We calculated GLCM with an inter-pixel distance of 1 and with 3×3 window size band by band. 8 filters include mean, variance, homogeneity, contrast, dissimilarity, entropy, second moment, and correlation were chosen to calculate the candidate GLCM. Finally the most representative GLCM were decided as the key spatial factors for uncertainty estimation using the pure and non-pure training data extracted from PPI and the logistic regression model.

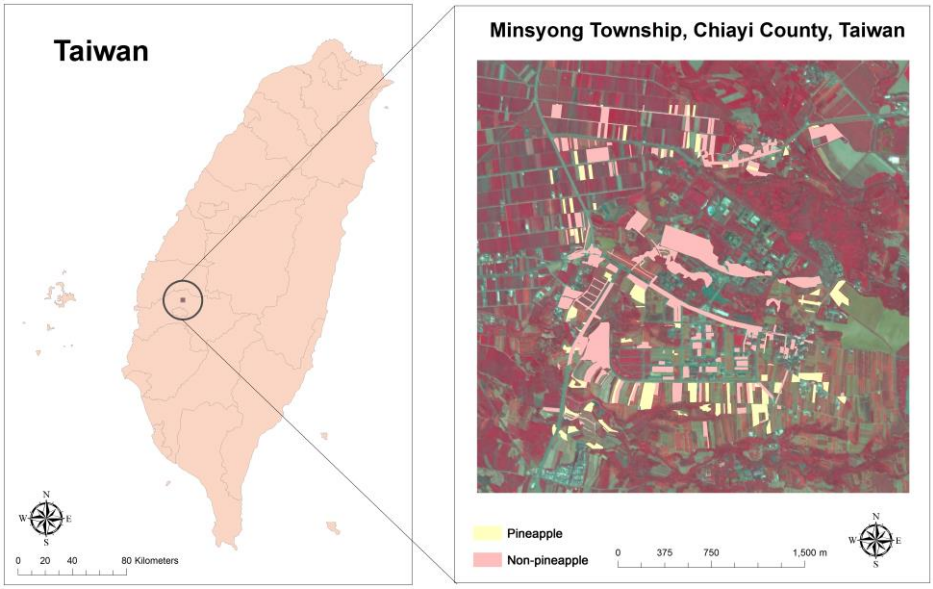

Fig. 1 Study area in Central Taiwan.

2.3 Uncertainty Estimation of Training Sites

With the selected GLCM from the logistic regression model, the WoE model was then used to estimate the uncertainty of training site selection. The uncertainty map can help decide the best training sites for image classification. A detailed description of WoE is available in Bonham-Carter et al. (2013). The method calculates the weight for each representative GLCM (G) based on the presence or absence of the best training sites (T) within the area as follows (Bonham-Carter et al., 2013; Dahal et al., 2008):

$$\mathrm{W}_{\mathrm{i}}^{+} = \ln \frac{P\{G \mid T\}}{P\{G \mid \overline{T}\}}, \tag{1}$$

$$\mathrm{W}_{\mathrm{i}}^{-} = \ln \frac{P\{\overline{G} \mid T\}}{P\{\overline{G} \mid \overline{T}\}}; \tag{2}$$

where P is the probability and ln is the natural log. Similarly, G is the presence of a given representative GLCM, $\overline{G}$ is the absence of a given representative GLCM, T is the presence of the best training sites and $\overline{T}$ is the absence of the best training sites. A positive weight (W_i^+) indicates that the predictable variable is present at the best training site locations and the magnitude of this weight is an indication of the positive correlation between the presence of the representative GLCM and the best training sites. A negative weight (W_i^-) indicates the absence of the representative GLCM and shows the level of negative correlation. The difference between the two weights is known as the weight contrast, W_f ($W_f = W_i^+ - W_i^-$); the magnitude of the contrast reflects the overall spatial association between the representative GLCM and the best training sites. To evaluate the contribution of each factor towards the best training

sites, the layer of best training sites was compared to various GLCM layers separately. For this purpose, Eqs. (1) and (2) were written in a number of pixel format as follows:

$$W_i^+ = \ln \frac{\frac{\mathrm{N}pix_1}{Npix_1 + Npix_2}}{\frac{\mathrm{N}pix_3}{Npix_3 + Npix_4}}, \quad (3)$$

$$W_i^- = \ln \frac{\frac{\mathrm{N}pix_2}{Npix_1 + Npix_2}}{\frac{\mathrm{N}pix_4}{Npix_3 + Npix_4}}; \quad (4)$$

where $Npix_1$ is the number of pixels representing the presence of both a given representative GLCM and the best training sites, $Npix_2$ is the number of pixels representing the presence of the best training sites and absence of a given representative GLCM, $Npix_3$ is the number of pixels representing the presence of a given representative GLCM and absence of the best training sites, $Npix_4$ is the number of pixels representing the absence of both a given representative GLCM and the best training sites.

2.4 Image Classification

Based on the hybrid approach, with both unsupervised and supervised classification, a pixel-based as well as geographic information system (GIS) object-based post classification (GOBPC) process was carried out (Shiu et al., 2012; Turner and Congalton, 1998). The hybrid approach utilized ISODATA (iterative self-organizing data analysis) and maximum likelihood classification techniques to overcome the high spectral heterogeneity and overlap caused by high land fragmentation in the study areas. In GOBPC, the cadastral parcel data were used as the classification unit. The class of a parcel was determined by using GIS zonal statistics and the pixel-based classification results. If half of the pixels covering one parcel are pineapple, then the parcel is assigned to the pineapple class, and vice versa.

3. RESULTS, DISCUSSION

3.1 Selection of the Representative GLCM

According to the pure and non-pure training data from PPI and the logistic regression model, the GLCM with p-values smaller than 0.05 were selected as the representative GLCM. The list of representative GLCM and their p-values was shown in Table 1. The results demonstrated that Band 1 (green) of SPOT-5 and its derivative GLCM have significant relationship with the pixel purity. Among the 8 GLCM indexes, second moment has the most significant relationship with the pixel purity.

Table 1 The list of representative GLCM and their p-values

Representative GLCM	p-value
Mean of Band 1	1.06×10^{-05}
Homogeneity of Band 1	6.59×10^{-19}
Dissimilarity of Band 1	9.32×10^{-12}
Second Moment of Band 1	7.61×10^{-06}
Second Moment of Band 2	9.95×10^{-06}
Second Moment of Band 4	3.08×10^{-02}
Correlation of Band 1	2.25×10^{-35}

3.2 Uncertainty Estimation for Training Site Selection

Like most uncertainty estimation approaches, the generalization of the factors with reclassification is inevitable because of the basic assumption of the models (Aboye, 2009; Lan et al., 2004; Pourghasemi et al., 2012). To be more objective, we reclassified each representative GLCM into 5 classes with natural-breaks (Jenk) method, which can

minimize within-class variance and maximized between-class variance in an iterative series of calculations (Jenks and Coulson, 1963). Class 1 stands for the area with the lowest GLCM values while class 5 represents the highest. According to the Eqs. (3) and (4), W_i^+, W_i^- and W_f of each class of each representative GLCM were calculated. The summary of the evidence classes identified as indicators for the best training sites is shown in Table 2. High W_f value indicates the given class of the given GLCM has high positive correlation with the presence of the best training sites, and vice versa. After calculating the W_f value for each representative GLCM, the uncertainty estimation map for training site selection can be generated by summing up all W_f value layers. As Fig. 2 shows, ROC curve and AUC imply that the WoE model performance is in "excellent" class according to the quantitative-qualitative relationship between AUC and prediction accuracy (Pourghasemi et al., 2012). The uncertainty estimation map was classified into five levels: five potential levels, very low, low, uncertain, high and very high potential based on the natural-breaks method. Compared the original image in Fig. 1 and the uncertainty estimation map in Fig. 3, vegetation generally shows higher potential level while roads and bare soil surfaces commonly exhibit lower level. As we assumed, several pineapple fields show lower potential level because of the mixed spectra from the mixture of pineapple plants and soil.

3.3 WoE Model Assessment with Image Classification

Different training sites were selected for image classification based on the uncertainty estimation map. The curves in Fig. 4 show the relationship between different potential level of training sites and the corresponding accuracy assessment results. According to the literature, purer and more homogeneous training sites make better classification results. However, the facts show the purest and most homogeneous training sites can only contribute the highest producer's accuracy of pineapple and user's accuracy of non-pineapple. Generally, the best classification results come from the mid-pure and mid-homogeneous training sites. The above results are different from the findings of the previous study (Shao and Lunetta, 2012). The main reason may come from the inevitable highly-mixed nature of each 2.5-meter pixel in a pineapple field. Pure and homogeneous training sites can only help classify the pure and homogeneous pineapple fields while cannot classify most pineapple fields with mixed spectra. Furthermore, the very high AUC 0.988 also indicates the possible problem of overfitting. And, last but not least, this study did not consider the number of pixels of training sites as one of the selection criteria, which has been suggested to be larger than $10n$ pixels for each class with an n-band image (Jensen, 2005).

4. CONCLUSIONS

This study provides an alternative solution for training site selection. Future applications include providing the best and minimum training sites and maximizing the accuracy of image classification. Yet, future studies may have to focus on three issues. First, this study classified the image into dual classes only including pineapple and non-pineapple. Accuracy assessment of classification with multiple classes is necessary for the most practical conditions. Second, the reclassification of each representative GLCM and the uncertainty estimation result would be a tricky step in the WoE model. Different reclassification method can lead different result. More objective substitute step has to be proposed to improve this uncertainty. Finally, methodologies of training site selection suitable for SVM or other classifiers are also necessary in practice.

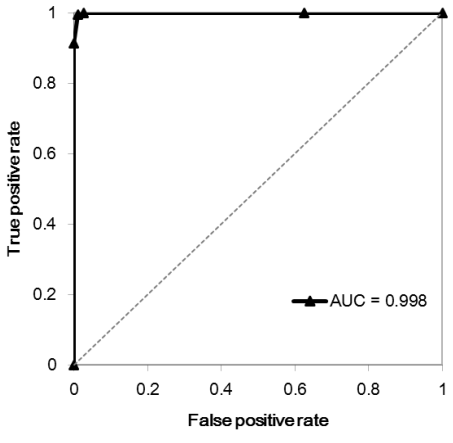

Fig 2 ROC curve and AUC of the WoE model.

Table 2 Summary of the evidence classes identified as indicators for the best training sites (only two of the representative GLCM are shown here).

GLCM	Class	*Npix1*	*Npix2*	*Npix3*	*Npix4*	W^+	W^-	W_f
Mean of Band 1	1	94	1089	16497	1919984	2.233	-0.074	2.307
	2	14	1169	298880	1637601	-2.568	0.156	-2.724
	3	5	1178	522206	1414275	-4.156	0.310	-4.466
	4	9	1174	798964	1137517	-3.993	0.524	-4.518
	5	1059	124	291593	1644888	1.783	-2.092	3.875
Dissimilarity of Band 1	1	873	310	475501	1460980	1.100	-1.057	2.158
	2	24	1159	829759	1106722	-3.050	0.539	-3.589
	3	1	1183	460431	1476050	-5.640	0.271	-5.911
	4	3	1180	146657	1789824	-3.397	0.076	-3.473
	5	281	902	15792	1920689	3.372	-0.263	3.635

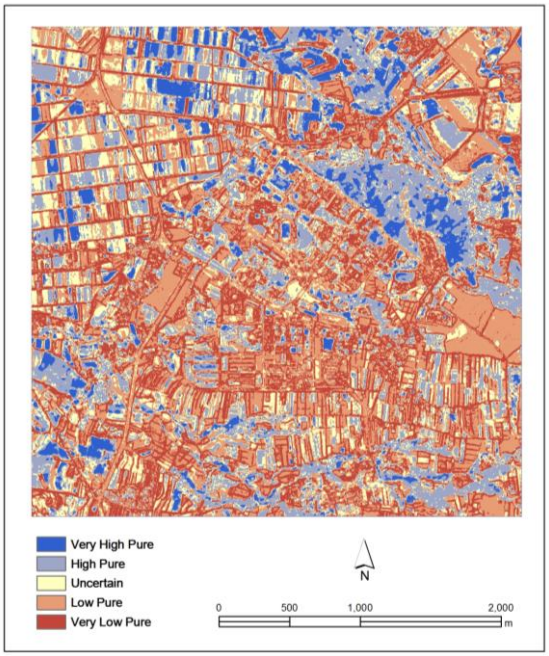

Fig. 3 Uncertainty estimation of training site selection generated from the WoE model.

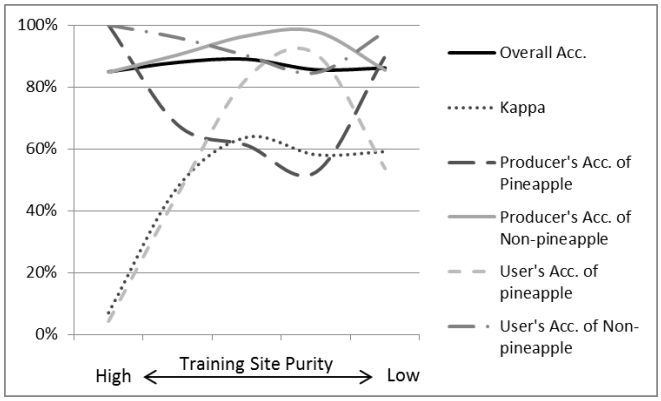

Fig. 4 Accuracy assessment of image classification using the training sites with different potential level.

5. REFERENCES

[1] Aboye, S.A., 2009. Slope stability analysis using GIS and numerical modeling techniques. In: Physical Land Resources (p. 145). Brussels: University Ghent.

[2] Binaghi, E., Luzi, L., Madella, P., Pergalani, F., and Rampini, A., 1998. Slope instability zonation: a Comparison between certainty factor and fuzzy Dempster–Shafer approaches. *Natural Hazards, 17*(1), pp. 77-97.

[3] Boardman, J.W., 1994. Geometric Mixture Analysis of Imaging Spectrometry Data. *IEEE International Geoscience & Remote Sensing Symposium, 4*, pp. 2369-2371.

[4] Bolstad, P.V., and Lillesand, T.M., 1992. Semi-automated training approaches for spectral class definition. *International Journal of Remote Sensing, 13*(16), pp. 3157-3166.

[5] Bonham-Carter, G.F., Agterberg, F.P., and Wright, D.F., 2013. Integration of Geological Datasets for Gold Exploration in Nova Scotia. *Digital Geologic and Geographic Information Systems* (pp. 15-23): American Geophysical Union.

[6] Buchheim, M.P., and Lillesand, T.M., 1989. Semi-Automated Training Field Extraction and Analysis for Efficient Digital Image Classification. *PHOTOGRAMMETRIC ENGINEERING AND REMOTE SENSING, 55*, pp. 1374-1355.

[7] Comber, A., Fisher, P., Brunsdon, C., and Khmag, A., 2012. Spatial analysis of remote sensing image classification accuracy. *Remote Sensing of Environment, 127*, pp. 237-246.

[8] Dahal, R., Hasegawa, S., Nonomura, A., Yamanaka, M., Masuda, T., and Nishino, K., 2008. GIS-based weights-of-evidence modelling of rainfall-induced landslides in small catchments for landslide susceptibility mapping. *Environmental Geology, 54*(2), pp. 311-324.

[9] Devkota, K., Regmi, A., Pourghasemi, H., Yoshida, K., Pradhan, B., Ryu, I., Dhital, M., and Althuwaynee, O., 2013. Landslide susceptibility mapping using certainty factor, index of entropy and logistic regression models in GIS and their comparison at Mugling–Narayanghat road section in Nepal Himalaya. *Natural Hazards, 65*(1), pp. 135-165.

[10] Foody, A.M.G.M., 2008. Crop classification by support vector machine with intelligently selected training data for an operational application. *International Journal of Remote Sensing, 29*, pp. 2227–2240.

[11] Foody, G.M., and Mathur, A., 2004. Toward intelligent training of supervised image classifications: directing training data acquisition for SVM classification. *Remote Sensing of Environment, 93*(1–2), pp. 107-117.

[12] Haralick, R.M., 1979. Statistical and structural approaches to texture. *Proceedings of the IEEE, 67*(5), pp. 786-804.

[13] Hiroshi Okumuraa, M.M.a.K.A., 2003. Appropriate training area selection for supervised texture classification by using the genetic algorithms, *4885*, pp. 411-420.

[14] Ifarraguerri, A., and Chein, I.C., 1999. Multispectral and hyperspectral image analysis with convex cones. *Geoscience and Remote Sensing, IEEE Transactions on, 37*(2), pp. 756-770.

[15]Jenks, G.F., and Coulson, R.C., 1963. Class intervals for statistical maps. *International Yearbook of Cartography, 3*, pp. 119-134.
[16] Jensen, J.R., 2005. *Introductory digital image processing: a remote sensing perspective*. (Third ed.). Upper Saddle River, N.J.: Prentice Hall.
[17] Lan, H.X., Zhou, C.H., Wang, L.J., Zhang, H.Y., and Li, R.H., 2004. Landslide hazard spatial analysis and prediction using GIS in the Xiaojiang watershed, Yunnan, China. *Engineering Geology, 76*(1-2), pp. 109-128.
[18] Mantero, P., Moser, G., and Serpico, S., 2004. Partially Supervised Classification of Remote Sensing Images through SVM-based Probability Density Estimation. *IEEE TRANSACTIONS ON GEOSCIENCE AND REMOTE SENSING, 43*(3), pp. 559-570.
[19] Martínez, P.J., Pérez, R.M., Plaza, A., Aguilar, P.L., Cantero, M.C., and Plaza, J., 2006. Endmember extraction algorithms from hyperspectral images. *ANNALS OF GEOPHYSICS, 49*, pp.
[20] Mccaffrey, T.M., and Franklin, S.E., 1993. Automated training site selection for large-area remote-sensing image analysis. *Computers & Geosciences, 19*, pp. 1413-1428.
[21] Mountrakis, G., and Xi, B., 2013. Assessing reference dataset representativeness through confidence metrics based on information density. *ISPRS Journal of Photogrammetry and Remote Sensing, 78*, pp. 129-147.
[22] Muñoz-Marí, J., Tuia, D., Camps-Valls, G., and Senior, 2012. Semisupervised Classification of Remote Sensing Images With Active Queries. *IEEE TRANSACTIONS ON GEOSCIENCE AND REMOTE SENSING, 50*, pp. 3751-3763.
[23] Ozdarici Ok, A., and Akyurek, Z., 2011. Automatic training site selection for agricultural crop classification: a case study on Karacabey Plain, Turkey. *International Archives of the Photogrammetry, Remote Sensing and Spatial Information Sciences, XXXVIII-4*, pp. 221-225.
[24] Pourghasemi, H., Pradhan, B., Gokceoglu, C., Mohammadi, M., and Moradi, H., 2012. Application of weights-of-evidence and certainty factor models and their comparison in landslide susceptibility mapping at Haraz watershed, Iran. *Arabian Journal of Geosciences*, pp. 1-15.
[25] Puissant, A., Hirsch, J., and Weber, C., 2005. The utility of texture analysis to improve per - pixel classification for high to very high spatial resolution imagery. *International Journal of Remote Sensing, 26*(4), pp. 733-745.
[26] Regmi, A., Devkota, K., Yoshida, K., Pradhan, B., Pourghasemi, H., Kumamoto, T., and Akgun, A., 2014. Application of frequency ratio, statistical index, and weights-of-evidence models and their comparison in landslide susceptibility mapping in Central Nepal Himalaya. *Arabian Journal of Geosciences, 7*(2), pp. 725-742.
[27] Shao, Y., and Lunetta, R.S., 2012. Comparison of support vector machine, neural network, and CART algorithms for the land-cover classification using limited training data points. *ISPRS Journal of Photogrammetry and Remote Sensing, 70*, pp. 78-87.
[28] Shiu, Y.-S., Lin, M.-L., Huang, C.-H., and Chu, T.-H., 2012. Mapping paddy rice agriculture in a highly fragmented area using a geographic information system object-based post classification process. *Journal of Applied Remote Sensing, 6*, pp. 063526.
[29] Sinha, A.P., and Zhao, H., 2008. Incorporating domain knowledge into data mining classifiers: An application in indirect lending. *Decision Support Systems, 46*(1), pp. 287-299.
[30] Skidmore, A.K., 1989. Unsupervised training area selection in forests using a nonparametric distance measure and spatial information. *International Journal of Remote Sensing, 10*, pp. 1133-1146.
[31] Tehrany, M.S., Pradhan, B., and Jebur, M.N., 2014. Flood susceptibility mapping using a novel ensemble weights-of-evidence and support vector machine models in GIS. *Journal of Hydrology, 512*, pp. 332-343.
[32] Turner, M.D., and Congalton, R.G., 1998. Classification of multi-temporal SPOT-XS satellite data for mapping rice fields on a West African floodplain. *International Journal of Remote Sensing, 19*(1), pp. 21-41.
[33] Winter, M.E., 1999. N-FINDR: an algorithm for fast autonomous spectral end-member determination in hyperspectral data,, pp. 266-275.
[34] Zhang, Z.J., Yang, Z.X., Zhang, P., Mao, Z.J., and Hao, J.Y., 2009. Hierarchical network-based safety assessment decision support system for thermal power plants. In: Networking, Sensing and Control, 2009. ICNSC '09. International Conference on (pp. 592-596). Okayama City, Japan